### Title

Uncovering the functional residues of Arabidopsis isoprenoid biosynthesis enzyme HDS




### Journal

Proceedings of the National Academy of Sciences of the United States of America, 117(1)

### ISSN

0027-8424



### Authors

Wang, Jin-Zheng
Lei, Yongxing
Xiao, Yanmei
et al.



### Publication Date

2020-01-07

### DOI

10.1073/pnas.1916434117

Peer reviewed

# Uncovering the functional residues of *Arabidopsis* isoprenoid biosynthesis enzyme HDS

Jin-Zheng Wang[a,1], Yongxing Lei[b,1], Yanmei Xiao[c], Xiang He[a], Jiubo Liang[a], Jishan Jiang[a], Shangzhi Dong[b], Haiyan Ke[a], Patricia Leon[d], Philipp Zerbe[c], Youli Xiao[b,2], and Katayoon Dehesh[a,2]

[a]Department of Botany and Plant Sciences, Institute of Integrative Genome Biology, University of California, Riverside, CA 92521; [b]Chinese Academy of Sciences (CAS) Key Laboratory of Synthetic Biology, CAS Center for Excellence in Molecular Plant Sciences, Institute of Plant Physiology and Ecology, Chinese Academy of Sciences, 200032 Shanghai, China; [c]Department of Plant Biology, University of California, Davis, CA 95616; and [d]Departamento de Biología Molecular de Plantas, Instituto de Biotecnología, Universidad Nacional Autónoma de México, 62210 Cuernavaca, México

Edited by Kenneth Keegstra, Michigan State University, East Lansing, MI, and approved December 5, 2019 (received for review September 20, 2019)

**The methylerythritol phosphate (MEP) pathway is responsible for producing isoprenoids, metabolites with essential functions in the bacterial kingdom and plastid-bearing organisms including plants and Apicomplexa. Additionally, the MEP-pathway intermediate methylerythritol cyclodiphosphate (MEcPP) serves as a plastid-to-nucleus retrograde signal. A suppressor screen of the high MEcPP accumulating mutant plant (*ceh1*) led to the isolation of 3 revertants (designated *Rceh1–3*) resulting from independent intragenic substitutions of conserved amino acids in the penultimate MEP-pathway enzyme, hydroxymethylbutenyl diphosphate synthase (HDS). The revertants accumulate varying MEcPP levels, lower than that of *ceh1*, and exhibit partial or full recovery of MEcPP-mediated phenotypes, including stunted growth and induced expression of stress response genes and the corresponding metabolites. Structural modeling of HDS and ligand docking spatially position the substituted residues at the MEcPP binding pocket and cofactor binding domain of the enzyme. Complementation assays confirm the role of these residues in suppressing the *ceh1* mutant phenotypes, albeit to different degrees. In vitro enzyme assays of wild type and HDS variants exhibit differential activities and reveal an unanticipated mismatch between enzyme kinetics and the in vivo MEcPP levels in the corresponding *Rceh* lines. Additional analyses attribute the mismatch, in part, to the abundance of the first and rate-limiting MEP-pathway enzyme, DXS, and further suggest MEcPP as a rheostat for abundance of the upstream enzyme instrumental in fine-tuning of the pathway flux. Collectively, this study identifies critical residues of a key MEP-pathway enzyme, HDS, valuable for synthetic engineering of isoprenoids, and as potential targets for rational design of antiinfective drugs.**

plastid | MEP pathway | HDS enzyme | MEcPP | retrograde signaling

Isoprenoids and their diverse group of derivatives are among the most ancient and essential classes of natural products present in all domains of life. These metabolites serve a broad range of biological functions, including respiration, growth and development, reproduction, photosynthesis, defense, and environmental sensing, as well as biotechnological applications including pharmaceuticals, flavors, fragrances, fuels, and more (1–4). These structurally diverse metabolites are synthesized from 2 universal 5-carbon building blocks (isopentenyl diphosphate [IPP] and its isomer dimethylallyl diphosphate [DMAPP]) derived from 2 distinct metabolic routes, the mevalonic acid (MVA) and methylerythritol phosphate (MEP) pathways (5, 6). Most Gram-negative bacteria, cyanobacteria, apicomplexan, and green algae exclusively use the MEP pathway; however, plants are the only organisms that have retained both biochemical routes compartmentalized in the cytosol (MVA) and plastids (MEP) (6–9). The MEP pathway is composed of 7 enzymes, starting with 1-deoxy-d-xylulose-5-phosphate synthase (DXS) catalyzing the first and one of the rate-limiting steps controlling flux through the pathway (10–12).

The MEP-pathway intermediate methylerythritol cyclodiphosphate (MEcPP) is an established bifunctional entity, serving the metabolic pathway for the production of IPP and DMAPP and functioning as a stress-specific plastid-to-nucleus retrograde signal (13). The retrograde signaling function of MEcPP was uncovered through a genetic screen and subsequent isolation of the high MEcPP-accumulating *Arabidopsis* mutant plant, *ceh1*, caused by a mutation in the hydroxymethylbutenyl diphosphate synthase (HDS; also known as GcpE or IspG [13]). HDS is a [4Fe–4S]-protein catalyzing the penultimate step in the MEP pathway that converts MEcPP into HMBPP [(*E*)-4-hydroxy-3-methylbut-2-enyl diphosphate] by reductive dehydroxylation via the [4Fe–4S] cluster (5, 14–17). Subsequent analyses established the MEcPP-mediated induction of selected nuclear stress response genes such as *hydroperoxide lyase* (*HPL*) and the salicylic acid (SA) biosynthesis gene *isochorismate synthase* (*ICS1*), and, by extension, the accumulation of SA in conjunction with other consequential developmental and metabolic aberrations (13, 18–21). To identify the components of MEcPP signaling, we performed a suppressor screen in search of revertants with fully or partially abolished *ceh1* phenotypes. This led to isolation of several suppressor lines with reduced MEcPP levels, herein designated as revertants of *ceh* (*Rceh*). Analyses of *Rceh* lines established the presence of intragenic mutations resulting in substitution of highly conserved amino acids, spatially positioned in the MEcPP binding pocket and the iron–sulfur cluster domain of the HDS enzyme. Intriguingly, lack of collinearity between the HDS

## Significance

**The MEP pathway is an essential and evolutionarily conserved metabolic route present in most pathogenic bacteria, plants, and malaria; and hence a target for discovery of agricultural and medical applications, and an engineering template for production of isoprenoids. The essential nature of this pathway and inherent intricacies associated with enzyme activity assays have hampered in vivo structure and functional analyses. Here, we report the suppressor screen leading to identification of 3 functionally conserved amino-acid residues positioned at the active site cavity and cofactor binding domain of the key MEP-pathway enzyme, HDS. The proposed roles of these residues in determining HDS enzyme activity and the MEP-pathway flux offer a platform for rational design of antiinfective drugs and synthetic engineering of isoprenoids.**

Author contributions: J.-Z.W., Yanmei Xiao, Youli Xiao, and K.D. designed research; J.-Z.W., Y.L., Yanmei Xiao, X.H., J.L., J.J., S.D., and H.K. performed research; P.L. contributed new reagents/analytic tools; J.-Z.W., Yanmei Xiao, H.K., P.Z., and Youli Xiao analyzed data; and K.D. wrote the paper.

The authors declare no competing interest.

This article is a PNAS Direct Submission.



[1]J.-Z.W. and Y.L. contributed equally to the work.

[2]To whom correspondence may be addressed. Email: ylxiao@sibs.ac.cn or kdehesh@ucr.edu.

This article contains supporting information online at https://www.pnas.org/lookup/suppl/doi:10.1073/pnas.1916434117/-/DCSupplemental.

First published December 26, 2019.

enzyme kinetics and the corresponding in vivo MEcPP levels led to the notion of involvement of MEcPP levels in modulating the MEP-pathway flux via feedback regulation of DXS enzyme abundance.

Collectively, this study reveals critical residues of the HDS enzyme that are instrumental in structure–function analyses, and marks valuable targets for antibiotic and antimalarial drug design and potential candidates for synthetic biology to engineer high-value products at economically viable levels.

## Results

**Suppressor Screen Uncovers the Functional Residues of HDS.** In the search for suppressors that fully or partially revert the aberrant phenotypes of *ceh1* (L703F substitution in HDS), we mutagenized the mutant using EMS and searched for revertants (*Rceh*) with larger stature than that of the *ceh1* (Fig. 1 *A* and *B*). Next, the larger plants were selected and analyzed for their MEcPP levels, SA content, and luciferase (LUC) activity driven by an otherwise stress-inducible *HPL* promoter (Fig. 1 *C–E*). The screen led to the isolation of 6 revertants designated *Rceh 175–6*, *6–2*, *13–7*, *181–2*, *147–15*, and *172–6*. The progeny of the crosses between these revertants and the *ceh1* mutant display dominant traits as the result of mutations in a gene tightly linked to *HDS*. Subsequent sequence analyses determined that the 6 revertants are caused by 3 intragenic mutations in the *HDS*, herein designated as *Rceh1* (C1648T; *175–6*), *Rceh2* (G1876A; *6–2*, *13–7*, *181–2*), and *Rceh3* (G4047A; *147–15* and *172–6*), without notable impact on *HDS* transcript levels (Fig. 1 *F* and *G*). The isolation of 3 independent revertants for *Rech2* versus 2 revertants for *Rceh3* and 1 for *Rceh1* reflects differential substitution frequencies per nucleotide and identifies G1876A as a mutation "hot spot" in the *HDS*. Moreover, revertants suppress *ceh1* aberrant phenotypes at varying degrees, with *Rceh1* displaying the least recovery and *Rceh3* showing wild type phenotypes (Fig. 1 *A–E*). Expression analyses exclude the contribution of the *HDS* transcript levels to gradation of the phenotypes observed, but rather to amino acid residue substitutions at the secondary site mutations in *Rech1* (A232V), *Rech2* (A282T), and *Rceh3* (D688N) lines (Fig. 1 *F* and *G*).

To confirm the function of the substituted amino acids in reverting the *ceh1* mutant phenotypes, we transformed *ceh1* with constructs containing the wild type and mutant variants of *HDS* encoding enzymes, namely *Rceh1* (L703F/A232V), *Rceh2* (L703F/A282T), and *Rceh3* (L703F/D688N). The similarity between phenotype recovery of the *Rceh* suppressor lines and the corresponding transgenic *ceh1*/*Rceh*-expressing *HDS* mutant variants verified the function of the secondary site mutations in altering HDS enzyme activity (Fig. 2 *A–E*).

**Spatial Positioning of Mutated Residues by Molecular Modeling.** To decipher the catalytic impact of the aforementioned mutated residues in the revertants, we combined a multisequence alignment of HDS sequences of diverse origin and structural modeling of the HDS protein using the established *Arabidopsis* HDS model structure (22).

Prior structural analyses of HDS enzymes have established the presence of 2 domains in bacterial IspGs: an N-terminal catalytic TIM barrel domain (A) and a C-terminal 4Fe-4S reductase domain (B) (23–26). However, HDS enzymes in some photosynthetic green sulfur bacteria, algae, mosses, and plants, as well as in numerous pathogens such as *Babesia bovis*, *Theileria parva*, *Chlamydia*, and malaria parasites, contain a second TIM barrel (A*) inserted between the A and B domains, which functions primarily as a structural domain (22). Structural modeling of *Arabidopsis* HDS and ligand docking placed MEcPP within the TIM barrel structure of the A-domain and supported a diphosphate linkage between MEcPP and R185, K281, and R342. These 3 residues are strictly conserved across known members of the enzyme family and discerned to be involved in ligand binding of bacterial HDSs (16, 27). In addition, the observed binding

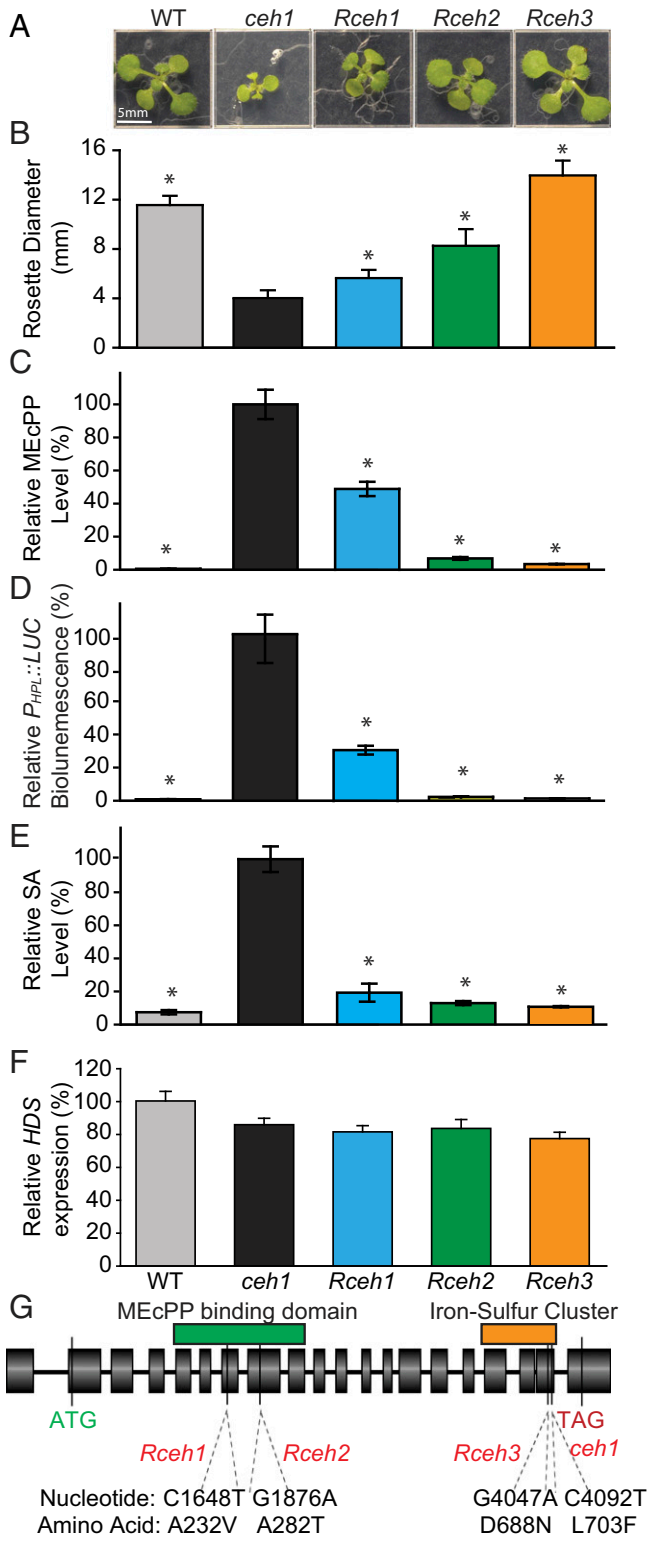


**Fig. 1.** Intragenic mutations in HDS differentially revert the *ceh1* mutant phenotypes. (*A*) Representative images of 11-d-old wild type (WT), *ceh1*, *Rceh1*, *Rceh2*, and *Rceh3* plants and (*B*) the corresponding average rosette diameters. Data are means ± SEM ($n \geq 20$). (*C*) Relative levels of MEcPP, (*D*) relative $P_{HPL}$::*LUC* activity, (*E*) SA levels, and (*F*) expression levels of *HDS* in aforementioned genotypes. Data are means ± SEM ($n \geq 4$). Asterisks indicate significance ($P < 0.05$). (*G*) Schematic of *HDS* gene structure with solid boxes representing exons, the green rectangle displaying MEcPP binding domain, and the orange rectangle showing the iron-sulfur cluster domain of the HDS. The mutants are noted in red letters, and their respective nucleotide and amino acid changes are displayed underneath.

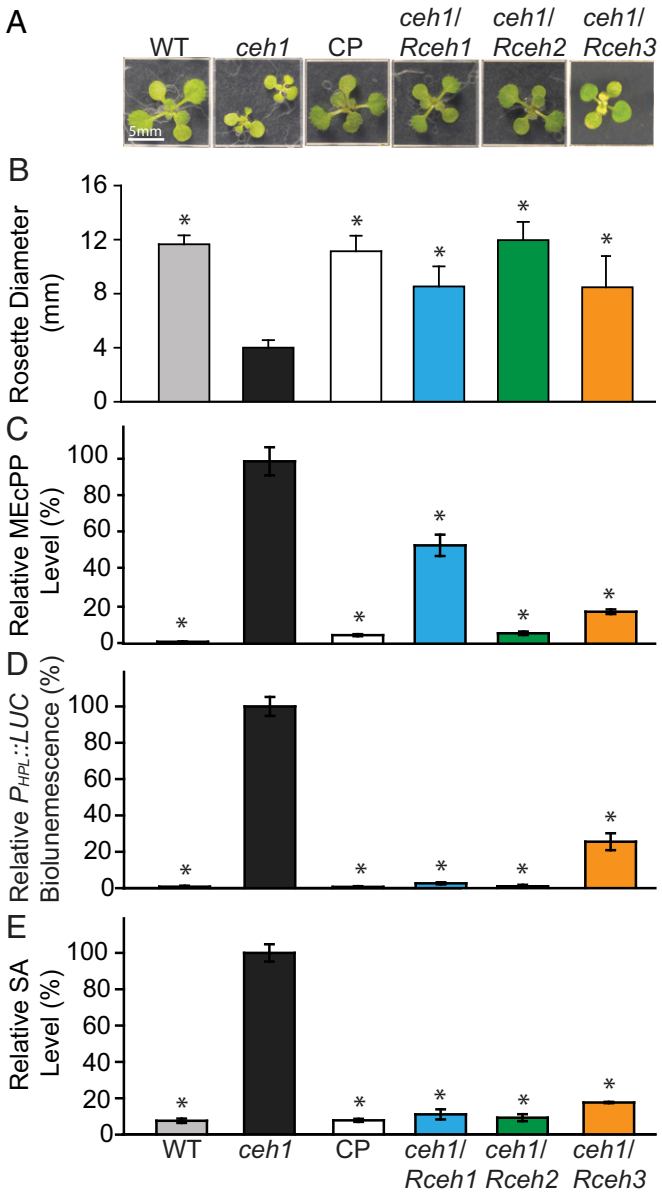


**Fig. 2.** Complementation analyses confirm HDS functional residues. (*A*) Representative images of 11-d-old wild type (WT), *ceh1*, transgenic *ceh1*-expressing wild type (complemented; CP), and mutated HDS, namely *ceh1/Rceh1*, *ceh1/Rceh2*, and *ceh1/Rceh3*. (*B*) Average rosette diameters of aforementioned genotypes. Data are means ± SEM ($n \geq 20$). (*C*) Levels of MEcPP, (*D*) $P_{HPL}$::*LUC* activity, and (*E*) SA relative to *ceh1*. Data are means ± SEM ($n \geq 4$). Asterisks indicate significance ($P < 0.05$).

pattern was consistent with ligand interactions previously reported for HDS (IspG) enzymes from *Aquifex aeolicus* and *Thermus thermophilus* (22, 24, 27).

Using the generated HDS model, we spatially positioned the residues identified to differ between the revertant HDS variants (Fig. 3 *A* and *B*). All focal mutants, A232V, A282T, D688N, and L703F, were placed in the catalytically relevant A- and B-domains. Among these, L703F resides at the center of the B-domain and D688N is placed at the interface of the B- and A-domains, both in relative proximity to the Fe-S cluster (Fig. 3*B*). Residues A232V and A282T are positioned at the bottom and at the top of the catalytic TIM barrel, respectively (Fig. 3*B*), suggesting that the respective substitutions A232V (*Rech1*) and A282T (*Rech2*) may alter substrate binding affinities.

Recovery of *ceh1* mutant phenotype was most notable in *Rceh3* (D688N/L703F) mutant background. The modeling studies positions D688 at the interface between the TIM barrel and the B-domain (Fig. 3*B*), suggesting a possible role in mediating the conformational change impacting HDS catalytic activity upon substrate binding.

The data collectively support the functionality of the identified residues in substrate binding and catalytic activity of the HDS enzyme.

**Enzymatic Characterization of HDS Variants.** To gain insights into the relative contribution of the aforementioned functional residues to HDS catalytic activity, we conducted in vitro enzyme activity assays using recombinant protein variants. To enhance expression of *HDS* variants and the solubility of the respective recombinant enzymes, we codon-optimized the wild type *HDS* and used it as a template for generating HDS mutant variants (L703F, L703F/A232V, L703F/A282T, and L703F/D688N). These constructs were introduced into *Escherichia coli*, and recombinant proteins were recovered. The in vitro activity assays with purified enzymes showed differential catalytic properties ($k_{cat}/k_m$) among the tested variants. As expected, the wild type was the most active enzyme, followed by ranks of activities showing *Rceh3* (L703F/D688N) > *Rceh1* (L703F/A232V) > *Rceh2* (L703F/A282T) > *ceh1* (L703F; Fig. 4, Table 1, and *SI Appendix*, Fig. S1). Specifically, relative enzyme activities of mutant variants to the wild type HDS are 39% (*Rceh3*), 1.5% (*Rceh2*), 5% (*Rceh1*), and 0.5% (*ceh1*).

Activity assays with protein variants containing A232V and A282T substitutions in combination with the L703F mutation showed increased substrate binding as compared to enzymes carrying only the L703F substitution, along with similar or slightly higher $k_m$ values as compared to the wild type enzyme (Fig. 4, Table 1, and *SI Appendix*, Fig. S1). Furthermore, higher activity of D688N/L703F compared to L703F variants may point to a possible role of D688 in conformational change at the interface between the TIM barrel and the B-domain impacting catalytic activity upon substrate binding.

The data collectively confirm the relevance of the secondary site mutations in enhancing *ceh1* (L703F) enzyme activity, with L703F/D688N as the most active and L703F/A282T as the least active enzyme variants.

**Differential DXS Enzyme Abundance in Revertants.** The discordance between notable recovery of the *ceh1* aberrant phenotypes in *Rceh2* despite the low catalytic activity of the encoded enzyme as compared to the other 2 revertants led us to examine the abundance of the first (DXS) and the penultimate (HDS) enzymes of the MEP pathway that represent the known key rate-limiting steps in isoprenoid biosynthesis (Figs. 1 *A–E*, 4, and 5*A*).

Initially we performed quantitative PCR analyses to examine potential changes in expression levels of *DXS* in various genotypes (*SI Appendix*, Fig. S2). These data show no significant changes in the *DXS* transcript levels in the wild type and mutant backgrounds. Next, we performed immunoblot analyses to examine the protein levels using DXS antibody (Fig. 5*B*). The results illustrate differential DXS protein levels in various genotypes, specifically enhanced DXS protein abundance in *ceh1* and *Rceh1* as compared to levels present in wild type, *Rceh2*, and *Rceh3* lines (Fig. 5*B*). In contrast, immunoblot analyses using HDS antibody show similar HDS protein levels in *Rceh2* compared with the other 2 revertants (Fig. 5*C*). These data exclude differential HDS enzyme abundance as the reason for the discordance between Rceh2 activity and the phenotype recovery of the corresponding suppressor line, and identify DXS abundance as a factor contributing to reduced MEcPP levels in *Rceh2*. Furthermore, higher DXS abundance in *ceh1* and *Rceh1* lines positively correspond to their enhanced MEcPP levels compared to the other genotypes, potentially because of the increased flux through the MEP pathway.

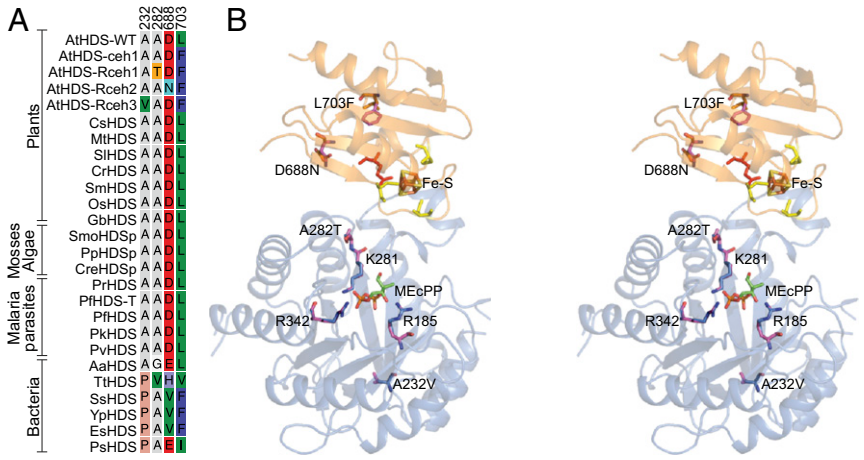


**Fig. 3.** Sequence comparison and structural modeling of HDS. (*A*) Multiple sequence alignment (bacterial kingdom and plastid-bearing organisms including plants and apicomplexans) and *Arabidopsis* mutants with relevant amino acid substitutions. The homology depicts broadly conserved residues substituted in *Rceh* mutants. (*B*) Cross-eyed stereo view of the homology model of the AtHDS B-domain (orange) and A-domain (blue) with MEcPP (green) docked insight the TIM barrel (A-domain) opening. Highlighted are residues R185, K281, and R342 involved in binding MEcPP, the CCCE motif coordinating the Fe-S cluster in the B-domain, as well as L703F, D688N, A282T, and A232V as mutated residues in the analyzed *Rceh* revertants (highlighted in magenta).

Collectively, the data exhibit a positive correlation between DXS protein abundance and high MEcPP levels in lines with compromised HDS enzyme activity, further supporting the key role of DXS as the first and a limiting step in the overall regulation of the pathway.

## Discussion

The MEP pathway is an evolutionarily conserved and indispensable biochemical route producing isoprenoids in plastid-bearing organisms and most Gram-negative bacteria, but is absent in animals and fungi. Intriguingly, environmental stimuli such as oxidative stress, high temperatures, and heavy metals result in reduced HDS enzyme activity, and, by extension, accumulation of one of the MEP-pathway intermediates, MEcPP, a bifunctional entity serving as a precursor of isoprenoids and a stress-specific retrograde signaling metabolite coordinating expression of selected nuclear stress response genes (13, 20, 21, 28–31). The key physiological function of MEP-pathway products and their absence in animals has led to targeting of the pathway for the development of antiinfective drugs as well as engineering of an array of biotechnological products and agronomic traits (1–4, 31). The successful implementation of these endeavors requires detailed structure–function analyses of the pathway enzymes, specifically the rate-limiting enzyme HDS (13, 31). However, these analyses have been restricted, given the essential nature of the pathway and inherent intricacies associated with in vivo and/or in vitro enzyme activity assays.

Use of a genetic screen aimed at the identification of suppressors of the high MEcPP-accumulating mutant *ceh1* resulted in the uncovering of 3 essential amino acid substitutions in the respective HDS variants that were subsequently verified using complementation studies. In vitro activity assays using recombinant protein variants revealed distinct catalytic activities, with *ceh1* being the least and *Rceh3* the most active enzyme compared to the wild type HDS.

Consistent with the observed catalytic impact, molecular modeling of HDS placed these residues within the A- and B-domains. Although docking of MEcPP in the open (nonactive) conformation of the B-domain did not allow a precise understanding of the mechanisms underlying the reduced HDS activity upon exchange of L703 to F, the position of L703 at the center of the B-domain may suggest that its substitution with a larger aromatic side chain may alter domain interactions and consequentially impact coordination with the Fe–S cluster. Under such circumstances, it may be speculated that L/F substitution can affect the side chain orientation of M686 and the neighboring E685. The latter is essential for coordinating the Fe–S cluster and substrate binding in bacterial IspGs (16, 23). For example, in the *T. thermophilus* IspG, the corresponding E350 binds to the Fe–S cluster and is replaced by the substrate (16). It is of note that a few bacterial IspG (HDS) enzymes such as *Yersinia pestis*, *Enterobacter* spp., and *Serratia* spp., naturally contain an F instead of an L residue at this position 703, which could point toward differences in catalysis of the dimeric compared to the monomeric enzyme in eukaryotic plastid-bearing organisms.

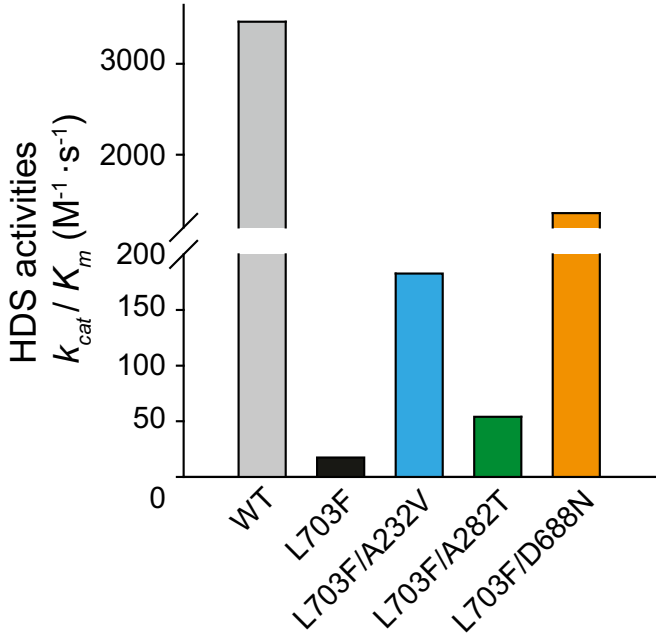


**Fig. 4.** Enzymatic characterization of HDS variants. In vitro enzyme activity assays of wild type (WT) and HDS mutant variants L703F (*ceh1*), L703F/A232V (*Rceh1*), L703F/A282T (*Rceh2*), and L703F/D688N (*Rceh3*) with MEcPP as the substrate show the corresponding catalytic efficiency ($k_{cat}/k_m$) values.

**Table 1. Summary of wild type and mutant HDS (IspG) steady-state kinetic data at 37 °C with MEcPP as substrate and MV/DT as chemical reduction system, respectively**

| Enzyme | $k_{cat}$, $min^{-1}$ | $K_m$, μM | $k_{cat}/K_m$, $M^{-1}•s^{-1}$ | $k_{cat}/K_m$ of WT-HDS, % |
|---|---|---|---|---|
| WT | 111 ± 11.15 | 533.7 ± 116 | 3,466 | 100 |
| L703F | 0.40 ± 0.02 | 383.4 ± 68.4 | 17.4 | 0.50 |
| L703F/A232V | 8.10 ± 1.53 | 739.2 ± 269.5 | 183 | 5.27 |
| L703F/A282T | 2.12 ± 0.41 | 654.9 ± 256.4 | 54 | 1.56 |
| L703F/D688N | 28.5 ± 2.77 | 350.1 ± 89.8 | 1,357 | 39.1 |

The assay was described in *Methods*. Data are means ± SD ($n$ = 3).

Moreover, placement of residue substitutions A232V (*Rceh1*) A282T (*Rceh2*) at the bottom and at the top of the catalytic TIM barrel, respectively, suggest possible roles in substrate binding. Interestingly, however, the respective higher binding affinities of the 2 variants relative to wild type enzyme does not extend to enhanced catalytic activities. Indeed, the reduced HDS activity is most notable in Rceh2, and yet, despite such a reduced enzyme activity, *Rceh2* suppressor lines accumulate less MEcPP as compared to *Rceh1*. This discordance could be explained by modified abundance of DXS enzyme as a key determinant of the flux through the MEP pathway by a yet-unknown mechanism. Intriguingly, the positive correlation between MEcPP accumulation and DXS enzyme levels in lines with compromised HDS activity suggest a potential MEcPP-mediated regulatory feedback mechanism to adjust the flux through this highly environmentally responsive pathway. Indeed, reduced HDS enzyme activity and the consequential enhanced MEcPP levels in response to myriad environmental signals, such as oxidative stress, high temperatures, and heavy metals (13, 20, 21, 28–31), may require fine-tuning of the MEP-pathway flux via altered de novo synthesis or stability of DXS enzyme abundance through MEcPP-mediated regulatory mechanism(s). This hypothesis is further supported by the reported transcriptional and posttranslational regulation of DXS in response to fluctuations in environmental and developmental conditions (32–34). The data from this study, however, suggest MEcPP-mediated posttranslational regulation of DXS and its potential function in fine tuning of the MEP-pathway flux. This notion is particularly supported by the role of HDS enzyme in limiting the kinetic capacity of the MEP pathway, and by the potential engagement of HDS and its substrate MEcPP in posttranscriptional regulation (17, 35). Indeed, a recent report on degradation of DXS by Clp protease (36, 37) offers an intriguing target for MEcPP-mediated fine tuning of the MEP-pathway flux.

The present report identifies 3 key functional residues of HDS involved in altering the activity of this key enzyme and sheds light on potential function of MEcPP as a rheostat for modification of DXS abundance geared toward ultimate control of the MEP-pathway flux in response to environmental cues. Furthermore, identification of these functional residues offers a platform for rational design of antiinfective drugs and synthetic engineering of economically viable levels of high-value isoprenoid products.

## Methods

**Plant Materials and Growth Condition.** The *Arabidopsis* mutant *ceh1* and its parent line harbor a $P_{HPL}$::*LUC* reporter gene in *Columbia-0* ecotype and were used in this study (13). The plants were grown at 20 °C at night and 23 °C during the day with a 16 h/day photoperiod.

**EMS Mutagenesis and Mutant Screening.** About 10,000 of *ceh1* seeds were subjected to mutagenesis as previously described using 0.2% EMS (vol/vol) (13, 38). M1 plants were grown in pools of ∼50 plants each, and a total of 20,000 M2 seeds from 206 pools were screened on plates containing 1/2 MS medium and the *ceh1* suppressors. *Rceh* plants were selected based on the plant size. Subsequent sequence analyses identified intragenic mutations in the *HDS* responsible for suppression of *ceh1* mutant phenotype.

**Complementation Test.** The *HDS* genes amplified from the individual *Rceh* mutants using the primers HDS-CP-FP and HDS-CP-RP (*SI Appendix*, Table S1) were cloned and subcloned to into Gateway Entry Vector pENTR/D-TOPO and the Gateway destination vector pFast-RO7, respectively (39). Upon sequence verification, the constructs were introduced into *Agrobacterium tumefaciens* strain GV3101 for transformation using the floral dip method

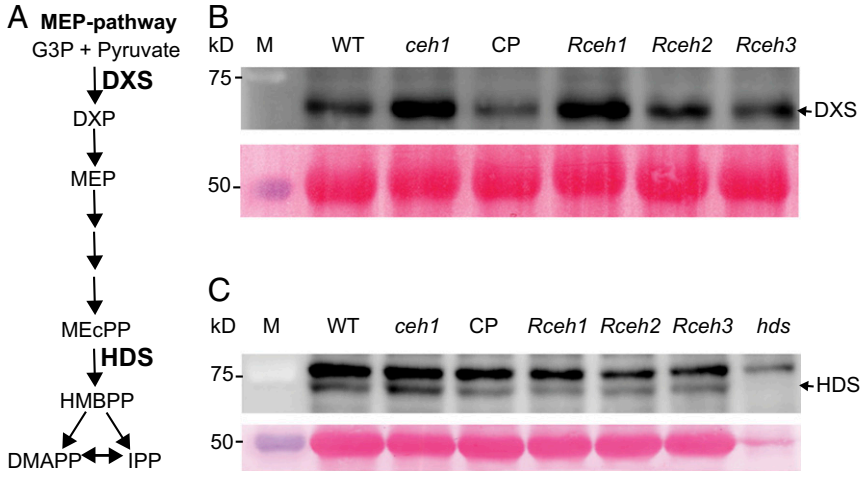


**Fig. 5.** Differential DXS enzyme abundance in revertants. (*A*) Schematic of the MEP pathway depicting DXS as the first and HDS the penultimate enzyme in isoprenoid biosynthetic pathway. Abundance of DXS (*B*) and HDS (*C*) proteins in total protein extracts from 2-wk-old WT, *ceh1*, CP, *Rceh1*, *Rceh2*, and *Rceh3* seedlings. Blots were probed with DXS (*B*) and HDS (*C*) antibodies, and Ponceau S (PS) staining was used as the protein loading control. The arrow in *C* shows the positions of HDS protein assessed using *hds* T-DNA insertion line. Sizes of markers are shown on the left.

(40). Selection of transgenic lines was based on the seed coat fluorescence (39), following confirmation by sequence analyses.

**Gene Expression.** The expression analyses were performed by quantitative real time-PCR (qRT-PCR), and *At4g34270* and *At4g26410* were used as the internal controls for transcript normalization as previously described (41), using primers listed in *SI Appendix*, Table S1.

**Quantification of SA and MEcPP.** Free SA level measurements were carried out by gas chromatography-mass spectrometry (GC-MS) as previously described (38) using deuterated SA as internal standard. MEcPP analysis was carried out using LS-MS as previously described (9, 19, 38) with deuterated MEcPP as internal standard.

**Protein Sequence Analyses.** Multiple sequence alignments of AtIspG (HDS) and the corresponding mutants were generated using the CLCbio Main Workbench software (https://www.qiagenbioinformatics.com/) with default parameters. Abbreviations are as follows: CsHDS, *Camellia sinensis* 4-hydroxy-3-methylbut-2-en-1-yl diphosphate synthase (HDS; K7PRX9); MtHDS, *Medicago truncatula* HDS (G7IRR3); SlHDS, *Solanum lycopersicum* HDS (Q8GZR6); CrHDS, *Catharanthus roseus* HDS (Q84XR5); SmHDS, *Salvia miltiorrhiza* HDS (H6VLE4); OsHDS, *Oryza sativa* HDS (Q6K8J4); GbHDS, *Ginkgo biloba* HDS (A9CBE3); SmoHDSp, *Selaginella moellendorffii* putative HDS (D8RQF1); PpHDSp, *Physcomitrella patens* putative HDS (A9RPA1); CreHDSp, *Chlamydomonas reinhardtii* putative HDS (Q4VKB7); PrHDS, *Plasmodium reichenowi* HDS (CDO64659); PfHDS-T, *Plasmodium falciparum* Tanzania HDS (A0A024W5X6); PfHDS, *P. falciparum* CAMP/Malaysia HDS (A0A024X6V3); PkHDS, *Plasmodium knowlesi* strain H HDS (A0A384KV27); PvHDS, *Plasmodium vivax* Sal-1 HDS (A5KE60); AaHDS, *A. aeolicus* HDS (O67496); TtHDS, *T. thermophilus* HDS (Q72H18); PsHDS, *Pseudomonas* sp. Ag1 HDS (EJF68563); SsHDS, *Serratia* sp. Ag1 HDS (KFK97316); YpHDS, *Yersinia pestis* strain IP275 HDs (EDR33568); and EsHDS, *Enterobacter* sp. Ag1 HDS (EJF30183).

**Chemoenzymatic Synthesis of MEcPP.** MEcPP was chemoenzymatically prepared from fructose-1,6-diphosphate (F-1,6-BP) as starting material using DXP pathway enzymes, DXS, IspC, IspD, IspE, IspF, TPI, and ALDO, with a modified reported method (*SI Appendix*, Method S1) (42).

**Codon Optimization and Purification of Recombinant HDS Enzyme Variants.** Gene encoding the wild type *Arabidopsis* HDS was codon-optimized and synthesized by Sunny (Shanghai, China). The DNA fragment was subcloned into the BamHI and XhoI sites of pET28b vector (*SI Appendix*, Method S2 and Table S2) herein designated pET28a-HDS. HDS variants with point mutations were cloned by QuikChange site-directed mutagenesis protocol using the primers shown in Table S2 and pET28a-HDS as a template. The constructs were transformed into BL21 (DE3) for IPTG inducible protein production. Protein purifications were conducted anaerobically in a Coy chamber using Ni-resin with the optimized protocol described in *SI Appendix*, Method S2 (42).

**In Vitro Activity Assays of HDS Enzyme Variants.** The kinetic study of HDS and mutants were conducted anaerobically in a Coy chamber with a modified protocol using the chemoenzymatically synthesized MEcPP as the substrate (*SI Appendix*, Methods S2 and S3 and Table S1) (42). All of the enzyme kinetics were determined with the chemically reduced methyl viologen as the artificial reductant (*SI Appendix*, Method S3)

**Structural Modeling and Ligand Docking.** Homology models of the A- and B-domains of relevant AtHDS protein variants were generated using SWISS-MODEL (43) based on the structural model of wild type AtIspG (provided by Eric Oldfield, Center for Biophysics and Computational Biology, University of Illinois, Urbana, IL). Obtained models were subjected to energy minimization with the YASARA force field (44) and validated for stereochemical correctness on the basis of Ramachandran plots showing greater than 97% of residues in allowed regions. Ligand docking was performed using the Molegro Virtual Docker software (https://www.qiagenbioinformatics.com/) with an energy-minimized MEcPP structure prepared using the PRODRG server (45) and subsequent visualization in PyMOL.

**Protein Extraction and Immunoblot Analyses.** Total proteins were extracted from 2-wk-old seedlings ground in liquid nitrogen and suspended in protein extraction buffer (PBS, pH 7.4, 100 mM NaCl, 1 mM EDTA, 10% glycerol, 0.5% Triton X-100) supplemented with EDTA-free Protease Inhibitor Mixture (Roche). The lysate was kept on ice for 30 min and occasionally vortexed before centrifugation at 16,000 × *g* for 15 min. Subsequently, protein samples were resolved on 8% SDS/PAGE and then transferred onto PVDF membrane (Millipore). Membranes were probed with DXS and HDS antibodies diluted in PBST at 1:2,000 and 1:1,500, respectively. The secondary antibodies conjugated to horseradish peroxidase (HRP) were anti-mouse for DXS (1:5,000) and anti-rabbit for HDS (1:3,000). Proteins were detected by applying enhanced chemiluminescence reagents (Thermo Scientific) and imaged by a ChemiDoc MP Imaging System (Bio-Rad).

**Statistical Analyses.** All experiments were performed with at least 3 biological replicates. Data are mean ± SEM. The analyses were carried out via 2-tailed Student's *t* tests with a significance of $P < 0.05$.

**Data Availability Statement.** All data discussed in the paper will be made available to readers.

**ACKNOWLEDGMENTS.** The authors thank Mr. S. Bu in the Core Facility Centre of the Institute of Plant Physiology and Ecology for assistance with NMR. This work was supported by the Chinese Academy of Sciences (CAS; Grants XDB27020203, 153D31KYSB20170121, and 153D31KYSB20160074 to Youli Xiao); UC Mexus Grant A01723 69085 44 OAD3 to P.L. and K.D.; and the Ernst and Helen Leibacher Endowment and NIH Award R01GM107311 to K.D.

1. N. Dudareva, E. Pichersky, Metabolic engineering of plant volatiles. *Curr. Opin. Biotechnol.* **19**, 181–189 (2008).
2. S. Tippmann, Y. Chen, V. Siewers, J. Nielsen, From flavors and pharmaceuticals to advanced biofuels: Production of isoprenoids in Saccharomyces cerevisiae. *Biotechnol. J.* **8**, 1435–1444 (2013).
3. C. E. Vickers, M. Bongers, Q. Liu, T. Delatte, H. Bouwmeester, Metabolic engineering of volatile isoprenoids in plants and microbes. *Plant Cell Environ.* **37**, 1753–1775 (2014).
4. C. E. Vickers, J. Gershenzon, M. T. Lerdau, F. Loreto, A unified mechanism of action for volatile isoprenoids in plant abiotic stress. *Nat. Chem. Biol.* **5**, 283–291 (2009).
5. M. Seemann *et al.*, Isoprenoid biosynthesis through the methylerythritol phosphate pathway: The (E)-4-hydroxy-3-methylbut-2-enyl diphosphate synthase (GcpE) is a [4Fe-4S] protein. *Angew. Chem. Int. Ed. Engl.* **41**, 4337–4339 (2002).
6. E. Vranová, D. Coman, W. Gruissem, Network analysis of the MVA and MEP pathways for isoprenoid synthesis. *Annu. Rev. Plant Biol.* **64**, 665–700 (2013).
7. Y. Hoshino, E. A. Gaucher, On the origin of isoprenoid biosynthesis. *Mol. Biol. Evol.*, 10.1093/molbev/msy120 (2018).
8. B. M. Lange, T. Rujan, W. Martin, R. Croteau, Isoprenoid biosynthesis: The evolution of two ancient and distinct pathways across genomes. *Proc. Natl. Acad. Sci. U.S.A.* **97**, 13172–13177 (2000).
9. E. E. Baidoo, Y. Xiao, K. Dehesh, J. D. Keasling, Metabolite profiling of plastidial deoxyxylulose-5-phosphate pathway intermediates by liquid chromatography and mass spectrometry. *Methods Mol. Biol.* **1153**, 57–76 (2014).
10. J. M. Estévez, A. Cantero, A. Reindl, S. Reichler, P. León, 1-Deoxy-D-xylulose-5-phosphate synthase, a limiting enzyme for plastidic isoprenoid biosynthesis in plants. *J. Biol. Chem.* **276**, 22901–22909 (2001).
11. J. Muñoz-Bertomeu, I. Arrillaga, R. Ros, J. Segura, Up-regulation of 1-deoxy-D-xylulose-5-phosphate synthase enhances production of essential oils in transgenic spike lavender. *Plant Physiol.* **142**, 890–900 (2006).
12. L. P. Wright *et al.*, Deoxyxylulose 5-phosphate synthase controls flux through the methylerythritol 4-phosphate pathway in Arabidopsis. *Plant Physiol.* **165**, 1488–1504 (2014).
13. Y. Xiao *et al.*, Retrograde signaling by the plastidial metabolite MEcPP regulates expression of nuclear stress-response genes. *Cell* **149**, 1525–1535 (2012).
14. M. Seemann, B. Tse Sum Bui, M. Wolff, M. Miginiac-Maslow, M. Rohmer, Isoprenoid biosynthesis in plant chloroplasts via the MEP pathway: Direct thylakoid/ferredoxin-dependent photoreduction of GcpE/IspG. *FEBS Lett.* **580**, 1547–1552 (2006).
15. M. Seemann *et al.*, Isoprenoid biosynthesis in chloroplasts via the methylerythritol phosphate pathway: The (E)-4-hydroxy-3-methylbut-2-enyl diphosphate synthase (GcpE) from Arabidopsis thaliana is a [4Fe-4S] protein. *J. Biol. Inorg. Chem.* **10**, 131–137 (2005).
16. F. Quitterer *et al.*, Atomic-resolution structures of discrete stages on the reaction coordinate of the [Fe4S4] enzyme IspG (GcpE). *J. Mol. Biol.* **427**, 2220–2228 (2015).
17. W. C. Chang, H. Song, H. W. Liu, P. Liu, Current development in isoprenoid precursor biosynthesis and regulation. *Curr. Opin. Chem. Biol.* **17**, 571–579 (2013).
18. M. J. Gil, A. Coego, B. Mauch-Mani, L. Jorda, P. Vera, The Arabidopsis csb3 mutant reveals a regulatory link between salicylic acid-mediated disease resistance and the methyl-erythritol 4-phosphate pathway. *Plant J.* **44**, 155–166 (2005).
19. M. Lemos *et al.*, The plastidial retrograde signal methyl erythritol cyclopyrophosphate is a regulator of salicylic acid and jasmonic acid crosstalk. *J. Exp. Bot.* **67**, 1557–1566 (2016).
20. J. Walley *et al.*, Plastid-produced interorgannellar stress signal MEcPP potentiates induction of the unfolded protein response in endoplasmic reticulum. *Proc. Natl. Acad. Sci. U.S.A.* **112**, 6212–6217 (2015).
21. J. Z. Wang *et al.*, Initiation of ER body formation and indole glucosinolate metabolism by the plastidial retrograde signaling metabolite, MEcPP. *Mol. Plant* **10**, 1400–1416 (2017).

22. Y. L. Liu *et al*., Structure, function and inhibition of the two- and three-domain 4Fe-4S IspG proteins. *Proc. Natl. Acad. Sci. U.S.A.* **109**, 8558–8563 (2012).
23. M. Lee *et al*., Biosynthesis of isoprenoids: Crystal structure of the [4Fe-4S] cluster protein IspG. *J. Mol. Biol.* **404**, 600–610 (2010).
24. I. Rekittke, H. Jomaa, U. Ermler, Structure of the GcpE (IspG)-MEcPP complex from Thermus thermophilus. *FEBS Lett.* **586**, 3452–3457 (2012).
25. I. Rekittke *et al*., Structure of the E-1-hydroxy-2-methyl-but-2-enyl-4-diphosphate synthase (GcpE) from Thermus thermophilus. *FEBS Lett.* **585**, 447–451 (2011).
26. F. Zepeck *et al*., Biosynthesis of isoprenoids. purification and properties of IspG protein from Escherichia coli. *J. Org. Chem.* **70**, 9168–9174 (2005).
27. I. Rekittke, E. Warkentin, H. Jomaa, U. Ermler, Structure of the GcpE-HMBPP complex from Thermus thermophilius. *Biochem. Biophys. Res. Commun.* **458**, 246–250 (2015).
28. Z. Li, T. D. Sharkey, Metabolic profiling of the methylerythritol phosphate pathway reveals the source of post-illumination isoprene burst from leaves. *Plant Cell Environ.* **36**, 429–437 (2013).
29. D. Ostrovsky *et al*., Effect of oxidative stress on the biosynthesis of 2-C-methyl-D-erythritol-2,4-cyclopyrophosphate and isoprenoids by several bacterial strains. *Arch. Microbiol.* **171**, 69–72 (1998).
30. D. Ostrovsky *et al*., Synthesis of a new organic pyrophosphate in large quantities is induced in some bacteria by oxidative stress. *Biofactors* **3**, 261–264 (1992).
31. C. Rivasseau *et al*., Accumulation of 2-C-methyl-D-erythritol 2,4-cyclodiphosphate in illuminated plant leaves at supraoptimal temperatures reveals a bottleneck of the prokaryotic methylerythritol 4-phosphate pathway of isoprenoid biosynthesis. *Plant Cell Environ.* **32**, 82–92 (2009).
32. E. Cordoba, M. Salmi, P. León, Unravelling the regulatory mechanisms that modulate the MEP pathway in higher plants. *J. Exp. Bot.* **60**, 2933–2943 (2009).
33. A. Guevara-García *et al*., Characterization of the Arabidopsis clb6 mutant illustrates the importance of posttranscriptional regulation of the methyl-D-erythritol 4-phosphate pathway. *Plant Cell* **17**, 628–643 (2005).
34. M. Rodríguez-Concepción, A. Boronat, Breaking new ground in the regulation of the early steps of plant isoprenoid biosynthesis. *Curr. Opin. Plant Biol.* **25**, 17–22 (2015).
35. L. Zhao, W. C. Chang, Y. Xiao, H. W. Liu, P. Liu, Methylerythritol phosphate pathway of isoprenoid biosynthesis. *Annu. Rev. Biochem.* **82**, 497–530 (2013).
36. P. Pulido *et al*., Specific Hsp100 chaperones determine the fate of the first enzyme of the plastidial isoprenoid pathway for either refolding or degradation by the stromal Clp protease in Arabidopsis. *PLoS Genet.* **12**, e1005824 (2016).
37. J. C. Moreno *et al*., Temporal proteomics of inducible RNAi lines of Clp protease subunits identifies putative protease substrates. *Plant Physiol.* **176**, 1485–1508 (2018).
38. J. Jiang, L. Zeng, H. Ke, B. De La Cruz, K. Dehesh, Orthogonal regulation of phytochrome B abundance by stress-specific plastidial retrograde signaling metabolite. *Nat. Commun.* **10**, 2904 (2019).
39. T. L. Shimada, T. Shimada, I. Hara-Nishimura I, A rapid and non-destructive screenable marker, FAST, for identifying transformed seeds of Arabidopsis thaliana. *Plant J.* **61**, 519–528 (2010).
40. S. J. Clough, A. F. Bent, Floral dip: A simplified method for Agrobacterium-mediated transformation of Arabidopsis thaliana. *Plant J.* **16**, 735–743 (1998).
41. J. W. Walley *et al*., Mechanical stress induces biotic and abiotic stress responses via a novel cis-element. *PLoS Genet.* **3**, 1800–1812 (2007).
42. Y. Xiao, G. Zahariou, Y. Sanakis, P. Liu, IspG enzyme activity in the deoxyxylulose phosphate pathway: Roles of the iron-sulfur cluster. *Biochemistry* **48**, 10483–10485 (2009).
43. M. Biasini *et al*., SWISS-MODEL: Modelling protein tertiary and quaternary structure using evolutionary information. *Nucleic Acids Res.* **42**, W252–W258 (2014).
44. E. Krieger *et al*., Improving physical realism, stereochemistry, and side-chain accuracy in homology modeling: Four approaches that performed well in CASP8. *Proteins* **77** (suppl. 9), 114–122 (2009).
45. A. W. Schüttelkopf, D. M. van Aalten, PRODRG: A tool for high-throughput crystallography of protein-ligand complexes. *Acta Crystallogr. D Biol. Crystallogr.* **60**, 1355–1363 (2004).